

Lateral Fluid Forces on Whirling Centrifugal Impeller (2nd Report: Experiment in Vaneless Diffuser)

H. Ohashi

Professor,
Department of Mechanical Engineering,
University of Tokyo,
Bunkyo-ku, Tokyo, 113 Japan

H. Shoji

Lecturer,
Institute of Engineering Mechanics,
University of Tsukuba,
Ibaraki-ken, 305 Japan

Fluid forces acting on a rotating centrifugal impeller in whirling motion are studied experimentally. A two-dimensional impeller installed in a parallel walled vaneless diffuser was forced on a circular orbital motion at various positive and negative whirl speeds. The measurements show that the fluid forces exert a damping effect on the rotor at most operating conditions, but excite positive whirl when the impeller operates at a partial discharge and rotates at speeds more than twice the whirl speed. The test results were compared with those calculated by the theory described in the 1st Report. The characteristics of whirling fluid forces are examined from both the measurements and calculations. The measured fluid forces are expressed in terms of mass, damping, and stiffness matrices.

Introduction

The present paper represents the experimental counterpart of the theory described in the 1st Report (Shoji and Ohashi, 1987). The test impellers and casing geometries were chosen as simple as possible to clarify the nature of fluid forces on whirling centrifugal impellers through direct comparison with corresponding calculations.

In these tests, a two-dimensional centrifugal impeller with logarithmic-spiral vanes was installed in a parallel walled vaneless diffuser and forced into a whirling motion with a circular orbit. Only the lateral fluid forces acting on the impeller vanes were measured at various operating conditions. This was accomplished by a special test procedure which excluded all the other forces acting on the shrouds, shaft and seals. This enabled a direct comparison of experimental and theoretical results.

In the data analysis the measured lateral forces were divided into radial and tangential components relative to the orbital motion. The influences of impeller geometry, whirl speed ratio and flow condition (flow coefficient) on these components were then separately investigated. To facilitate the calculation of rotordynamic response to an unbalance mass or to seismic loads, the measured forces were converted to mass, damping and stiffness matrices by assuming that the forces are proportional to the acceleration, velocity and displacement of the impeller center.

The investigation of fluid forces on whirling centrifugal impellers was first approached analytically as described in the introduction of the 1st Report. The corresponding experimental studies on this problem are quite limited. Investigations similar to the present one have been carried out by Acosta et al. (Brennen et al., 1980; Chamieh et al., 1982 and 1985; Jery et al., 1984) for propellant-turbopump impellers and by

Bolleter and Wyss (1985) for boiler feed pump impellers. Their measurements were presented using the same expressions adopted in the present study. In the comparison of these results, attention must be paid to the difference of the whirling body of the interest, namely two-dimensional impeller vanes or a complete three-dimensional impeller with shrouds.

Test Setup

For the measurement of lateral fluid forces, a single-stage, vertical-shaft, centrifugal pump is used. As Fig. 1 shows, water is sucked from the tank to the impeller. The test impellers A and B differ only in their vane angles. Their geometries and the test parameters are given in Table 1. Each impeller is installed at the center of a parallel walled vaneless diffuser as illustrated in Fig. 2(b). The discharged water is decelerated in the diffuser and returns to the tank via two symmetrically arranged pipes. The flow rate of each pipe is ad-

Table 1 Principal specifications

Impeller	Two-dimensional, closed type
outer diameter $d_2=2r_2$	350 mm
inner diameter	175 mm
vane width b	35 mm
shroud thickness	5 mm × 2
number of vanes	6
vane angle to radius β (logarithmic spiral)	68° for impeller A 60° for impeller B
mass	4.1 kg
Vaneless diffuser	Parallel walled
exit diameter	700 mm
screen	40 mesh per inch, 51% opening
width	70 mm
Test condition	
rotational speed ω	525 rpm
whirl speed Ω	-683 to +683 rpm
eccentricity e	variable, mainly 1.5 mm
shock-free flow rate	2.25 m ³ /min for impeller A 3.21 m ³ /min for impeller B

Contributed by the Fluids Engineering Division for publication in the JOURNAL OF FLUIDS ENGINEERING. Manuscript received by the Fluids Engineering Division, January 30, 1986.

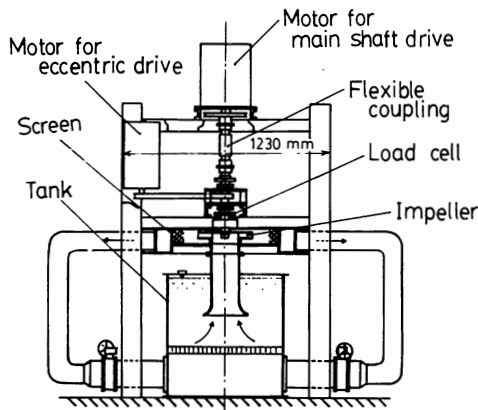
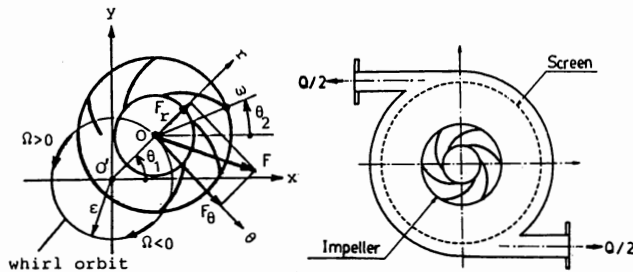


Fig. 1 Layout of test facility



(a) Impeller force

(b) Vaneless diffuser

Fig. 2 Fluid forces on whirling impeller

justed to be the same by flow control valves. In order to improve the diffuser flow uniformity, a screen (40 mesh per inch) is installed at the outer periphery of the diffuser. The pump discharge is measured by a flow nozzle at the suction pipe entrance.

The forced whirling motion apparatus is illustrated in Fig. 3. The impeller is supported overhung by two self-aligned spherical roller bearings and driven by an electric motor through a flexible coupling. The upper and lower bearings are supported by two auxiliary crankshafts with the same eccentricity, which are driven synchronously via a cogged belt connected to a variable speed electric motor. The rotating pump shaft can thus be forced into an orbital motion with a given whirl speed and eccentricity, while keeping its axis always parallel. To reduce the whirling motion resistance, a multi-disk shaft seal is installed. The wear ring on the front shroud is replaced by a teflon face seal with a narrow axial gap.

Lateral fluid forces on the impeller are evaluated from the

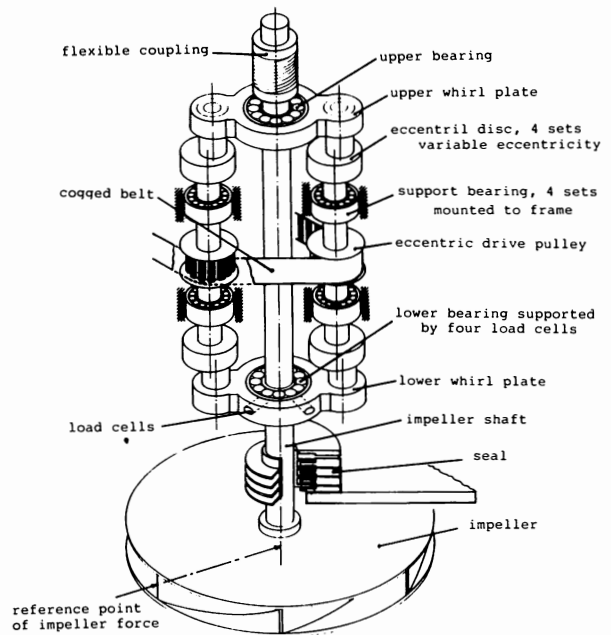


Fig. 3 Forced whirling motion apparatus

lower bearing reaction. As seen from Fig. 3, the outer race of this bearing is attached to the lower whirl plate by four load cells arranged orthogonally (x - and y -direction). The phase angles of whirl and rotation, θ_1 and θ_2 (see Fig. 2(a)), are recorded by rotary encoders attached to the auxiliary and main shafts. The rotational speed of the impeller ω is kept constant (525 rpm), while the whirl speed Ω is varied from negative to positive (-683 to $+683$ rpm) giving a wide range of whirl speed ratios ($-1.3 < \Omega/\omega < 1.3$).

Test Method

Calibration. The relation between load cell outputs and lateral forces working at the center of the vane width was obtained dynamically by rotating a dummy disk with a known unbalance mass. The x - and y -component of the calculated centrifugal force, F_x and F_y , are related to the load cell outputs, E_x and E_y , by the linear equation:

$$\begin{bmatrix} F_x \\ F_y \end{bmatrix} = \begin{bmatrix} a_{xx} & a_{xy} \\ a_{yx} & a_{yy} \end{bmatrix} \cdot \begin{bmatrix} E_x \\ E_y \end{bmatrix} \quad (1)$$

The four elements of the conversion matrix, \mathbf{a} , are deter-

Nomenclature

$\mathbf{a}(a_{xx}, \dots)$ = conversion matrix and their elements
 b = vane width
 \mathbf{b} = damping matrix
 $\mathbf{E}(E_x, E_y)$ = load cell output in x - and y -direction
 $\mathbf{F}(F_x, F_y)$ = fluid force in x - and y -direction
 f = normalized fluid force
 \mathbf{k} = stiffness matrix
 M = mass of fluid displaced by rotating vanes, $\rho\pi r_2^2 b$

M_a = apparent mass of impeller vanes
 \mathbf{m} = mass matrix
 n = number of data sampling
 Q = flow rate
 r_2 = outer radius of impeller
 S = standard deviation of sampled data
 u_2 = peripheral speed
 x, y = Cartesian coordinate
 Δp_t = total pressure rise
 β = vane angle

ϵ = eccentricity
 θ_1 = whirl angle
 θ_2 = rotational angle
 ν = kinematic viscosity
 ρ = fluid density
 ψ = head coefficient
 ϕ = flow coefficient
 Ω = whirl speed
 ω = rotational speed

Subscripts

r, θ = radial and tangential component to the orbit
 sf = shockfree entry condition

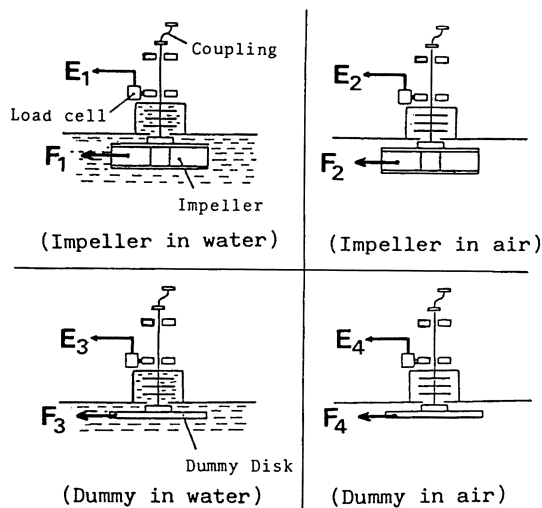


Fig. 4 Four sub-experiments

mined from calibration data collected at various rotational speeds using the least squares method. The interaction terms, a_{xy} and a_{yx} , between x - and y -direction were less than 2 percent of the principal terms, a_{xx} and a_{yy} . Therefore the impeller forces were evaluated using $F_x = a_{xx}E_x$ and $F_y = a_{yy}E_y$, neglecting small cross interaction.

Data Sampling. There is no impeller/guidevane interaction in this vaneless diffuser arrangement. Therefore the lateral force on a whirling impeller does not depend on the rotational angle θ_2 , as theory predicts for an impeller with 3 or more vanes (Shoji and Ohashi, 1987). If the vaneless diffuser created a perfectly unbounded condition for the impeller as expected, the fluid force on the impeller would also not depend on the whirl angle θ_1 . However in reality the fluid force varies with the whirl angle θ_1 due to the nonuniform flow at the diffuser exit as well as the slightly inhomogeneous rigidity of the whirling apparatus. In these tests the load cell outputs were sampled and A-D converted at each 10 degree increment of whirl angle resulting in 36 equally spaced locations on the orbit. At each location $n = 200 - 300$ sampling data were collected and their ensemble average was evaluated. To check the uncertainty of these ensemble averages, the standard deviation S of 512 sampling data were evaluated for several representative test conditions. A 95 percent confidence interval, $\pm 1.96 S/\sqrt{n}$, was then estimated. The uncertainty associated with the measuring system itself is negligible compared to the confidence interval caused by the force fluctuation.

Lateral Force on Impeller Vanes. When the impeller whirls in water, the resultant reaction force at the lower bearing is due to the following: the inertial (centrifugal) force acting on whirling body, the fluid force on the submerged parts including the shaft seal, the reaction force from the deformed flexible coupling, as well as the reaction force from the driving torque of non-aligned motor shaft. In order to extract the fluid force acting purely on the impeller vanes from the measured resultant force, four sub-experiments are carried out. They are shown in Fig. 4. First the whirling impeller is tested in water (output E_1) and in air (output E_2). Then the impeller is replaced by a dummy disk made up from the shrouds and hub of the original impeller, and the whirling test is again carried out in water (output E_3) and in air (output E_4).

The fluid forces on the impeller vanes, $F(F_x, F_y)$, can then be evaluated by the relation,

$$F = a(E_1 - E_2 - E_3 + E_4) \quad (2)$$

where $a(E_1 - E_2)$ represents fluid forces on all the submerged parts and $a(E_3 - E_4)$ those on the submerged parts other than

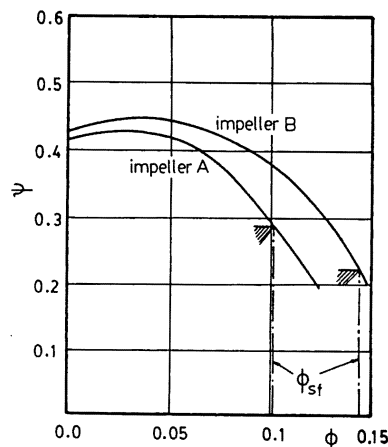


Fig. 5 Characteristics of test pump

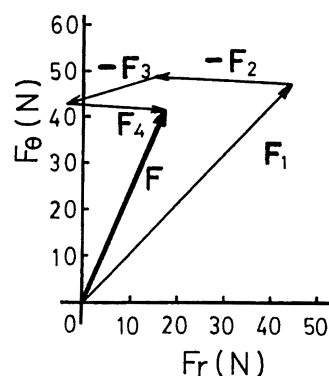


Fig. 6 Relative position of force vectors (impeller A, $\epsilon = 2.0$ mm, $\phi = \phi_{sf}$, $\Omega/\omega = 0.83$)

the impeller vanes. The reaction of driving torque on the lower bearing is calculated from the geometrical relation and the influence is corrected to the result obtained by equation (2). Hereafter fluid forces refer only to those on impeller vanes, unless otherwise specified.

Test Condition. Test parameters are listed in Table 1. Most of the tests were carried out for an eccentricity $\epsilon = 1.5$ mm, since preliminary tests showed that fluid forces were proportional to the eccentricity as long as it was sufficiently small compared to the impeller radius. The test flow rate was adjusted from shutoff to the maximum including shockfree entry condition. The machine Reynolds number was $Re = u_2 d_2 / \nu = 3.4 \times 10^6$ at constant rotational speed of 525 rpm.

Test Results

Pump Characteristics. The performance of the test pump was measured at steady operating conditions without whirl and was converted to flow and head coefficients by

$$\phi = Q/2\pi r_2 b u_2, \quad \psi = \Delta p_1 / (\rho u_2^2 / 2) \quad (3)$$

The pump characteristics are shown in Fig. 5 for impeller A and B. Impeller A with larger vane angle has correspondingly smaller shockfree flow coefficient ϕ_{sf} and smaller head than those of impeller B. The head of the test pump was generally smaller than that of an industrial pump with the same vane angle. This was due to additional losses at the sharp inlet corner of the two-dimensional test impeller and the presence of the resistance screen which reduced the net pressure rise.

Character of Unsteady Fluid Forces. The fluid forces on impeller vanes were derived from four sub-experiments in Fig. 4. The relative magnitude and direction of these forces are illustrated in Fig. 6 for a typical test condition (impeller A, Ω/ω

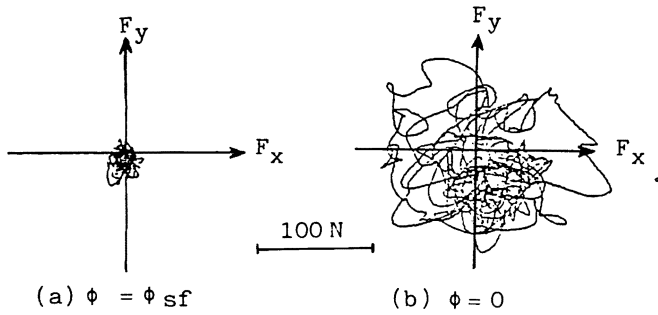


Fig. 7 Lissajous's figure of impeller force without whirling motion (Impeller A)

$= 0.83$, $\phi = \phi_{sf}$). The forces F_2 and F_4 measured in air are mostly due to the inertial centrifugal force and thus have a predominant radial component. The reduction of the whirling mass by using aluminum impeller helps to keep the magnitude of the fluid force substantially larger than that of the inertial force.

While the oscillatory output of load cells primarily correlates with the whirl speed Ω , it also contains secondary fluctuations caused by the mass unbalance of rotating impeller (frequency ω), the rolling noise of bearings, the turbulence of flow and so on. From the preliminary tests, it became clear that the largest and predominant source of secondary fluctuation resulted from the separation-induced flow disturbance. Figure 7 illustrates Lissajous's figures of overall impeller force, when impeller A rotates in water without whirling motion. As seen from Fig. 7(a) the fluctuation of measured force is rather weak at design condition corresponding to shockfree entry. As the discharge decreases, the fluctuation increases and becomes quite violent at shutoff as seen from Fig. 7(b). This strong fluctuation can be obviously attributed to the stall of impeller vanes at partial flow rate, where large eddies grow and mix randomly in the separated zones. From the spectrum analysis of measured data at partial flow rate, no distinct peak frequency was observed, which suggests that no orderly phenomena like propagating stall occurred in the impeller. The power of fluctuation in synchronism with the shaft rotation remained within one tenth of the power related to the whirling motion.

Figure 8 shows the variation of fluid force acting on whirling impeller vanes along the orbit. The vector at each location represents the ensemble average of 512 sampled data taken at that point. The fluctuation from the average is indicated by a circle with its rms value as its radius. Examples are shown for shockfree and shutoff conditions with positive and negative whirl, $\Omega/\omega = \pm 0.83$. Fluid forces are nearly axisymmetric and uniform on the circular orbit as expected. It is worthwhile to note that the rms fluctuation near shutoff can be several fold larger than its average and the fluid forces excite the whirling motion only at such extraordinary flow conditions. This will be treated in detail in the discussion.

Fluid Forces on Whirling Impeller. In spite of the precautions to establish an azimuthally uniform flow, the ensemble averaged force vectors on the orbit were not completely identical as shown in Fig. 8. Since the motion of whirling rotor is due to the impulse of the fluid force, the force components, $F_r(\theta_1)$ and $F_\theta(\theta_1)$, are hereafter averaged over one cycle of whirling motion, $\theta_1 = 0$ to 360 deg, and are denoted by \bar{F}_r and \bar{F}_θ . These forces are further normalized using the following definitions:

$$f_r = \bar{F}_r / M\epsilon\omega^2, \quad f_\theta = \bar{F}_\theta / M\epsilon\omega^2 \quad (4)$$

$$M = \rho\pi r_2^2 b$$

where M denotes the mass of fluid displaced by the envelope of rotating vanes.

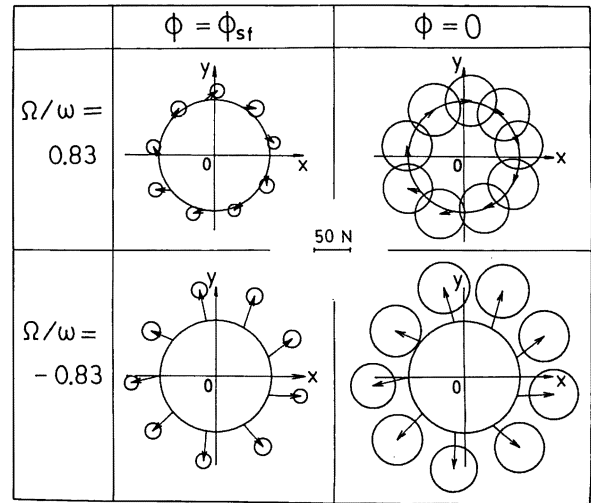


Fig. 8 Ensemble averaged fluid forces and their fluctuations (impeller A, $\epsilon = 1.5$ mm)

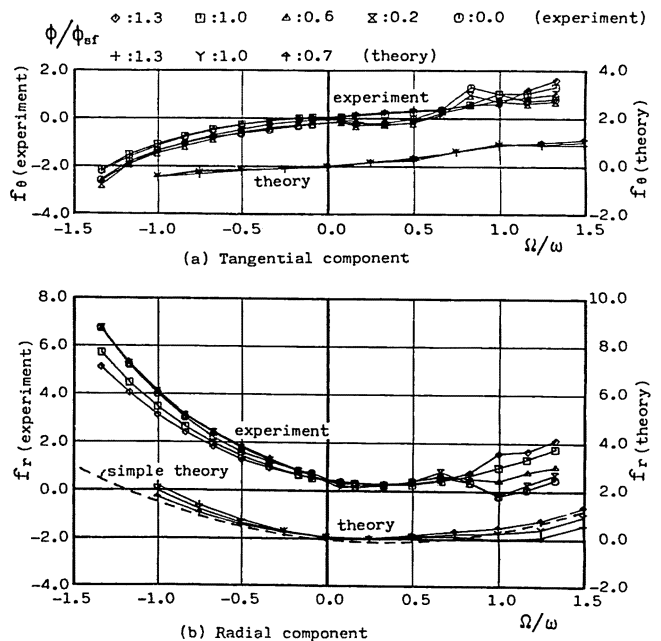


Fig. 9 Normalized fluid forces on impeller A (Uncertainty in f_θ and $f_r = \pm 0.10$ for \diamond , ± 0.17 for Δ , ± 0.21 for \circ . Uncertainty in $\Omega/\omega = \pm 0.02$ for all cases)

Figures 9(a) and (b) show the dependence of f_θ and f_r on the whirl speed ratio Ω/ω between -1.3 and $+1.3$. These results are for impeller A ($\beta = 68$ deg) whirling with eccentricity $\epsilon = 1.5$ mm at five different flow rates; $\phi/\phi_{sf} = 1.3, 1.0, 0.6, 0.2$, and 0 . The corresponding calculations are also plotted in the same figures. Figures 10(a) and (b) show the result for impeller B ($\beta = 60$ deg) at $\phi/\phi_{sf} = 1.0, 0.7, 0.4, 0.1$, and 0 .

The confidence intervals of measured fluid forces depend primarily on the flow coefficient and are slightly influenced by the whirl speed ratio. The uncertainties of force measurement are substituted in this case by the corresponding 95 percent confidence intervals and are given for representative flow coefficients in Figs. 9 and 10.

Fluid forces on whirling shrouds were determined from two sub-experiments using dummy disk whirling in water and in air. The results are normalized also by equation (3) with reference mass $M = \rho\pi r_2^2 t$ (where t is total thickness of front and back shrouds). The results are shown in Fig. 11.

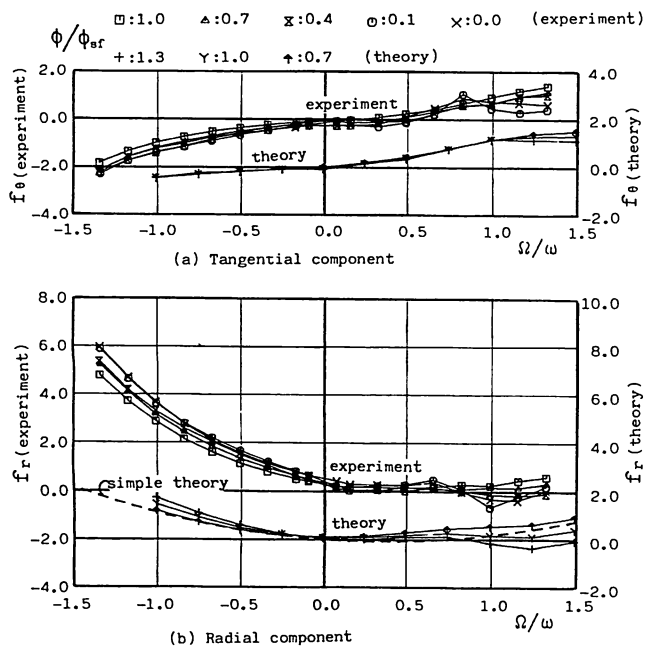


Fig. 10 Normalized fluid forces on impeller B (Uncertainty in f_θ and f_r =; ± 0.07 for \square , ± 0.14 for \bar{x} , ± 0.21 for X . Uncertainty in $\Omega/\omega = \pm 0.02$ for all cases)

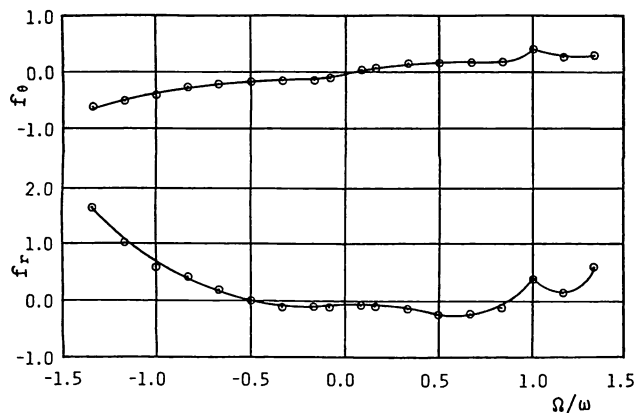


Fig. 11 Normalized fluid forces on shrouds (Uncertainty in f_θ and $f_r = \pm 0.10$, in $\Omega/\omega = \pm 0.02$)

Discussion of Results

Comparing the experimental results with the corresponding calculations, the character of whirling fluid forces could be clarified.

Tangential Forces.

(1) Normalized tangential forces f_θ increase on the whole with the increase of whirl speed ratio Ω/ω . Under most operating conditions except those described below, the tangential forces are positive for positive whirl and negative for negative whirl and exert a damping effect to the whirling motion.

The theoretical results show the same tendency. Quantitative agreement with the experiment is fairly good for positive whirl, while for negative whirl calculated damping is approximately half of the measured values.

(2) Tangential forces decrease slightly with the decrease of flow rate. Consequently, they become negative for positive whirl when both flow rate and whirl speed ratio are small, $\phi/\phi_{sf} < 0.6$ and $\Omega/\omega < 0.5$. From the viewpoint of rotor-dynamics, this indicates that the centrifugal impeller can excite positive whirl of the rotor, only when it is mounted on a flexi-

ble shaft rotating faster than twice its critical speed and operates at a partial flow rate near shutoff.

Comparison of impeller A and B indicates that impeller A with smaller head coefficient has a slightly wider excitation zone.

(3) Calculated f_θ is nearly zero at zero whirl speed ratio, $\Omega/\omega = 0$, or for a steady displacement of the impeller center. Therefore, the existence of excitation zone cannot be simulated using potential flow theory. In contrast the damping at most operating conditions can be predicted quantitatively.

(4) The mechanism of whirl-exciting tangential force is not clear. A clue could be found in the strong fluctuation of impeller force at partial flow rate. It is conceivable that the propagation of stall region in the impeller (usually about a half of the rotational speed) becomes synchronized with the whirling motion (also about a half or less) from time to time and this random fluctuation transfers positive energy to the whirling shaft stochastically. It seems that a potential flow theory is essentially powerless to explain the mechanism, since the flow in question is characterized by large separation and turbulence which are phenomena outside inviscid flow theory.

(5) Tangential force on whirling shrouds exerts always damping effect.

Radial Forces.

(1) Normalized radial forces f_r are smaller in positive whirl than in negative whirl. The distribution appears approximately parabolic with the minimum at about $\Omega/\omega = 0.4-0.5$. While there is qualitative agreement between theory and experiment, the measured values are 1.5 to 2 times larger than the calculated ones.

(2) In positive whirl f_r increases with increasing flow rate and in negative whirl an opposite tendency is observed. The same tendency is also observed in the calculation.

(3) Radial forces are positive or outwards acting in most cases. Negative radial forces occur at higher positive whirl speed ratio, $\Omega/\omega > 1$, and partial discharge. These characteristics are also present in the calculated results.

(4) When whirl speed coincides with rotational speed, $\Omega = \omega$, the relative flow in the whirling impeller becomes stationary and the shedding of free vortices from the trailing edges into the discharge flow disappears. Consequently the condition $\Omega/\omega = 1$ represents a singular flow condition and fluid forces, f_r as well as f_θ , exhibit irregular behavior around this point. This can be also seen in the calculated results.

(5) The condition $\Omega/\omega = 0$ corresponds to the case where the center of rotating impeller is statically displaced by eccentricity ϵ from the geometrical center of suction pipe. The radial forces are positive in this condition and act to further increase the displacement (negative spring).

(6) Impeller A with larger vane angle (hence longer vane) generates larger f_r values than impeller B, which agrees with the theoretical predictions.

(7) Radial forces are generated principally by the centrifugal force on the apparent mass of whirling impeller. Apparent mass of an impeller, M_a , in translatory oscillation without rotation can be calculated by potential flow theory. The result is given in Fig. 7 of the 1st Report for two-dimensional impellers with various vane numbers and angles. From this figure the apparent mass of impeller A is read as $M_a/M = 0.95$ and of impeller B as $M_a/M = 0.65$. Normalizing the centrifugal force of apparent mass, $M_a \epsilon \Omega^2$, using the reference force, $M \epsilon \omega^2$, results in a normalized radial force given by $f_r = (M_a/M) (\Omega/\omega)^2$. While this parabolic distribution is symmetric both to positive and negative whirl, it is not sufficient to explain the asymmetric distribution of the measured data.

When a body like impeller with circulation Γ travels on the orbit with velocity $\epsilon \Omega$, a lift $L = \rho \Gamma \epsilon \Omega b$ is supposedly generated according to the Kutta-Joukowski's theorem.

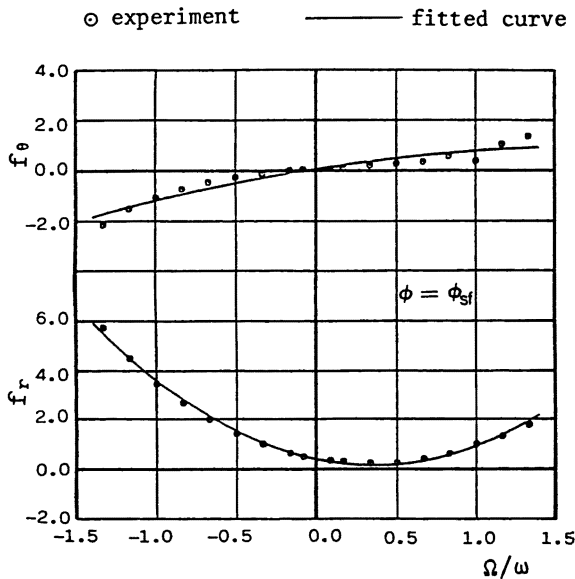


Fig. 12 Measured data and fitted curves of impeller A at shockfree entry condition (Uncertainty in f_θ and $f_r = \pm 0.07$, in $\Omega/\omega = \pm 0.02$)

Defining circulation in counterclockwise direction as positive, the impeller with positive whirl generates lift inwards corresponding to a negative radial force. Taking the absolute tangential velocity at the impeller exit as $v_{\theta 2}$, the circulation is $\Gamma = 2\pi r_2 v_{\theta 2}$ and the total pressure rise is given by $\Delta p_t = \psi(\rho u_2^2/2) = \rho u_2 v_{\theta 2} \eta$ (η is hydraulic efficiency). Normalizing this lift L by the same reference force, a linear relation $f_r = -(\psi/\phi)(\Omega/\omega)$ can be obtained. Combination of the above two forces leads to the following simplified equation for radial force:

$$f_r = (M_a/M)(\Omega/\omega)^2 - (\psi/\phi)(\Omega/\omega) \quad (5)$$

By substituting ϕ and ψ of impeller A and B at shockfree entry condition to the above equation, the impeller radial forces can be estimated and are plotted in Figs. 9 and 10 by broken curves. Since equation (5) does not account for the negative spring effect, the predicted distribution is a little smaller than the one by complete flow analysis. Nevertheless the overall relation between radial force and whirl speed can be adequately represented by equation (5).

(8) The radial force on whirling shrouds shows also the influence of lift. The rotating flow induced by disk friction causes a lift due to so-called Magnus effect.

Conversion to Force Matrices

For the vibration analysis of a rotor with centrifugal impellers, fluid forces must be formulated for an arbitrarily given motion of the shaft center. Although the experiment was carried out only for whirling motion with a circular orbit, the results can be generalized to an arbitrary shaft motion, if the forces are assumed to be proportional to the displacement, velocity and acceleration of the shaft center. Using absolute coordinate system with its origin at the whirl center O' (cf. Fig. 2(a)), x - and y -components of fluid forces, F_x and F_y , on impeller at $O(x, y)$ are expressed by the following relation with three linear terms:

$$\begin{bmatrix} F_x \\ F_y \end{bmatrix} = - \begin{bmatrix} m_{xx} & m_{xy} \\ m_{yx} & m_{yy} \end{bmatrix} \begin{bmatrix} \ddot{x} \\ \ddot{y} \end{bmatrix} - \begin{bmatrix} b_{xx} & b_{xy} \\ b_{yx} & b_{yy} \end{bmatrix} \begin{bmatrix} \dot{x} \\ \dot{y} \end{bmatrix} - \begin{bmatrix} k_{xx} & k_{xy} \\ k_{yx} & k_{yy} \end{bmatrix} \begin{bmatrix} x \\ y \end{bmatrix} \quad (6)$$

Table 2 Matrix elements of fluid forces on vanes

matrix element	m_{xx}, m_{yy}	$m_{xy}, -m_{yx}$	b_{xx}, b_{yy}	$b_{xy}, -b_{yx}$	k_{xx}, k_{yy}	$k_{xy}, -k_{yx}$	
normalized by	$\rho \pi r_2^2 b$		$\rho \pi r_2^2 b \omega$		$\rho \pi r_2^2 b \omega^2$		
impeller A	$\phi/\phi_{sf}=0$	1.64	-0.27	1.14	2.02	-0.55	0.13
	0.2	1.72	-0.35	1.10	2.01	-0.55	0.17
	0.6	1.87	-0.32	1.08	1.88	-0.56	0.10
	1.0	1.86	-0.27	0.98	1.33	-0.42	-0.09
	1.3	1.82	-0.23	1.09	1.01	-0.43	-0.08
impeller B	$\phi/\phi_{sf}=0$	1.30	-0.21	0.98	1.98	-0.58	0.12
	0.1	1.32	-0.33	0.94	1.96	-0.57	0.17
	0.4	1.26	-0.20	1.06	1.80	-0.43	0.13
	0.7	1.34	-0.19	1.01	1.62	-0.39	0.05
	1.0	1.32	-0.05	1.00	1.35	-0.35	-0.01

Table 3 Matrix elements of fluid forces on shrouds

matrix element	m_{xx}, m_{yy}	$m_{xy}, -m_{yx}$	b_{xx}, b_{yy}	$b_{xy}, -b_{yx}$	k_{xx}, k_{yy}	$k_{xy}, -k_{yx}$
normalized by	$\rho \pi r_2^2 t$		$\rho \pi r_2^2 t \omega$		$\rho \pi r_2^2 t \omega^2$	
$Q = 0$	0.67	-0.07	0.34	0.30	0.20	-0.01

where $x = \epsilon \cos \theta_1$, $y = \epsilon \sin \theta_1$ and $\theta_1 = \Omega t$.

The assumption that the fluid forces are identical at every location of the orbit, in other words, F_r and F_θ are constant and independent of whirl angle θ_1 in an unbounded vaneless diffuser, leads to the relations:

$$\begin{aligned} F_r(\epsilon, \Omega) &= \epsilon(F_{r0} + F_{r1}\Omega + F_{r2}\Omega^2) \\ F_\theta(\epsilon, \Omega) &= \epsilon(F_{\theta 0} + F_{\theta 1}\Omega + F_{\theta 2}\Omega^2) \end{aligned} \quad (7)$$

The six constants in the above equations are related to twelve unknown elements in three force matrices of equation (6) by

$$\begin{aligned} m_{xx} = m_{yy} &= F_{r2}, & m_{xy} &= -m_{yx} = F_{\theta 2} \\ b_{xx} = b_{yy} &= F_{\theta 1}, & b_{xy} &= -b_{yx} = -F_{r1} \\ k_{xx} = k_{yy} &= -F_{r0}, & k_{xy} &= -k_{yx} = -F_{\theta 0} \end{aligned} \quad (8)$$

All measured F_r and F_θ data over the entire whirl speed range, $-1.3 < \Omega/\omega < 1.3$, were fitted to equation (7) and the six constants, F_{r0} , F_{r1} , \dots , determined by the method of least squares. Figure 12 illustrates the good fit of these constants with the measured data for the case of impeller A at shockfree entry condition. As seen from this figure, the whirling fluid forces can be approximated by the linear relation of equation (7) satisfactorily ignoring the previously mentioned irregular behavior near $\Omega/\omega = 1$.

Normalized matrix elements for impeller A and B at various flow rates are summarized in Table 2.

The fitted curves of tangential force f_θ appear nearly linear to the whirl speed ratio. This implies from equation (8) that the cross mass term, $F_{\theta 2} = m_{xy} = -m_{yx}$, is small and has little effect (see Table 2). The radial force f_r , on the other hand, has a parabolic distribution with its minimum at around $\Omega/\omega = 0.4$ to 0.5 . This is obviously caused by the existence of a large principal mass term, $F_{r2} = m_{xx} = m_{yy}$, while the minimum is due to a large cross damping term, $F_{r1} = -b_{xy} = b_{yx} < 0$, resulting from the circulation-induced lift on the orbiting impeller.

The influence of tangential force f_θ on the stability of the rotor can be ascertained by the sign of f_θ at small whirl speed ratio, that is, by the sign of $F_{\theta 0} = -k_{xy} = k_{yx}$. If cross stiffness term k_{xy} is positive, the impeller excites positive whirl at higher supercritical rotational speed. From Table 2 it can be clearly seen that k_{xy} turns from negative (damping) to positive (exciting), as the discharge is decreased from design to partial flow rate.

Fluid forces on whirling shrouds can be also converted to matrix elements and they are listed in Table 3, where total thickness of shrouds, t , is used as the reference width instead of vane width b .

The matrix elements of impeller with an arbitrarily given vane width b and shroud thickness t , can be obtained by adding the impeller and shrouds matrix elements from Tables 2 and 3.

Conclusions

Fluid forces acting on two-dimensional centrifugal impeller whirling in a vaneless diffuser were measured and compared with the corresponding theoretical results. The principal results obtained from tests with two impellers are:

(1) Fluid forces have tangential components which damp the whirling motion at most operating conditions.

(2) In the case when impeller rotates faster than twice the critical speed and operates at partial flow rate, the tangential forces excite positive whirl and can induce an impeller-excited oscillation or impeller whip.

(3) The mechanism of radial force generation can be explained as the sum of an equivalent negative spring force acting against eccentricity, the circulation-induced lift on the orbiting impeller, and the centrifugal force on the apparent mass of the impeller.

(4) Calculated results agree with all measured data qualitatively. However, the mechanism of whirl-excitation cannot be explained by the inviscid theory used in the calculations.

(5) By assuming a linear relationship, whirling fluid forces are expressed in terms of mass, damping and stiffness matrices, separately for impeller and shrouds. This enables the formulation of fluid forces on impeller in an arbitrary motion.

In a future investigation, this study will be extended to treat the cases of two-dimensional impellers in a vaned diffuser and in a volute casing. This will be followed by the whirling test of industrial pumps such as a boiler feed pump.

Acknowledgments

This study was supported by the Japanese Ministry of Education through the Grant-in-Aid for Scientific Research. The authors express their deepest appreciation to Messrs. S. Yanagisawa, K. Tomita, J. Hanawa, K. Kawakami, and C. Kato for their assistance in the construction of test apparatus and in performing the measurements. The authors are also indebted to the Mechanical Engineering Research Laboratory of Hitachi, Ltd. for the continuous support and advice in this study. The authors are grateful to Dr. R. Latorre for his assistance in preparing the final manuscript.

References

- Bolleter, U., and Wyss, A., 1985, "Measurement of Hydrodynamic Interaction Matrices of Boiler Feed Pump Impellers," Paper 85-DET-148 presented at the ASME Design Engineering Division Conference.
- Brennen, C. E., Acosta, A. J., and Caughey, T. K., 1980, "A Test Program to Measure Fluid Mechanical Whirl-Excitation Forces in Centrifugal Pumps," NASA CP 2133, pp. 229-235.
- Chamieh, D. S., Acosta, A. J., Brennen, C. E., and Caughey, T. K., 1982, "Experimental Measurements of Hydrodynamic Stiffness Matrices for a Centrifugal Pump Impeller," NASA CP 2250, pp. 382-398.
- Chamieh, D. S., Acosta, A. J., Brennen, C. E., and Caughey, T. K., 1985, "Experimental Measurements of Hydrodynamic Radial Forces and Stiffness Matrices for a Centrifugal Pump-Impeller," ASME JOURNAL OF FLUIDS ENGINEERING, Vol. 107, No. 3, pp. 307-315.
- Jery, B., Acosta, A. J., Brennen, C. E., and Caughey, T. K., 1984, "Hydrodynamic Impeller Stiffness, Damping and Inertia in the Rotordynamics of Centrifugal Flow Pumps," NASA CP 2338, pp. 137-160.
- Shoji, H., and Ohashi, H., 1987, "Lateral Fluid Forces on Whirling Centrifugal Impeller (1st Report: Theory)," ASME JOURNAL OF FLUIDS ENGINEERING, published in this issue pp. 94-99.